Title

Micromotors for Active Delivery of Minerals toward the Treatment of Iron Deficiency Anemia

Journal

Nano Letters, 19(11)

ISSN

1530-6984

Authors

Karshalev, Emil
Zhang, Yue
de Ávila, Berta Esteban-Fernández
et al.

Publication Date

2019-11-13

DOI

10.1021/acs.nanolett.9b02832

Peer reviewed

Published in final edited form as:

Nano Lett. 2019 November 13; 19(11): 7816–7826. doi:10.1021/acs.nanolett.9b02832.

Micromotors for active delivery of minerals toward the treatment of iron deficiency anemia

Emil Karshalev[‡], **Yue Zhang**[‡], **Berta Esteban-Fernández de Ávila**[‡], **Mara Beltrán-Gastélum**, **Yijie Chen**, **Rodolfo Mundaca-Uribe**, **Fangyu Zhang**, **Bryan Nguyen**, **Yao Tong**, **Ronnie H. Fang**, **Liangfang Zhang**[*], **Joseph Wang**[*]

Department of NanoEngineering, University of California San Diego, La Jolla, CA 92093, USA.

Abstract

As the most common nutritional disorder, iron deficiency represents a major public health problem with broad impacts on physical and mental development. However, treatment is often compromised by low iron bioavailability and undesired side effects. Here, we report on the development of active mineral delivery vehicles using Mg-based micromotors, which can autonomously propel in gastrointestinal fluids, aiding in the dynamic delivery of minerals. Iron and selenium are combined as a model mineral payload in the micromotor platform. We demonstrate the ability of our mineral-loaded micromotors to replenish iron and selenium stores in an anemic mouse model after 30 days of treatment, normalizing hematological parameters such as red blood count, hemoglobin, and hematocrit. Additionally, the micromotor platform exhibits no toxicity after the treatment regimen. This proof-of-concept study indicates that micromotor-based active delivery of mineral supplements represents an attractive approach towards alleviating nutritional deficiencies.

Graphical Abstract

[*]**Corresponding Author**: Tel: 858-246-0128; josephwang@eng.ucsd.edu (J. W.), Tel: 858-246-0999; zhang@ucsd.edu (L.Z.).

Author Contributions

J.W., L.Z., E.K., Y.Z., and B.E.F-A. conceived the idea and designed the experiments. E.K., Y.Z., B.E.F-A., R.M-U., F.Z., M.B.-G., performed all the experiments. The manuscript was written by E.K., Y.Z., B.E.F-A., R.H.F., L.Z., and J.W. All authors contributed to the general discussion and reviewed the manuscript.

[‡]These authors contributed equally.

Supporting Information. The following files are available free of charge on the ACS Publications website at DOI: 10.1021/acs.nano-lett.

Enteric layer coating process, microscope and fluorescence images of loaded passive control particles, mouse weight after 30 days of treatment, calculation of daily recommended values and upper limits of minerals for mice (PDF), propulsion of non-loaded and mineral loaded micromotors (AVI).

The authors declare no competing financial interests.

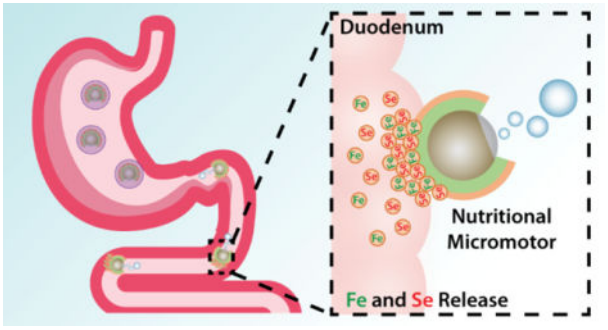

Keywords

anemia; nutrient deficiency; micromotor; active delivery; gastrointestinal absorption

Despite tremendous progress in growing and transporting food, a large fraction of the world population still suffers from severe nutritional deficiencies. While a variety of inorganic minerals are essential for regulating numerous metabolic pathways, iron (Fe) stands out as a crucial element for humans.[1–4] Fe deficiency represents the most common nutritional deficiency worldwide and has tremendous health and economic costs. Fe is vital in the transport of oxygen via hemoglobin, function of numerous enzymes responsible for biological oxidation, and gut microbiome health.[2,5] About one third of the world's population suffers from anemia, which represents a major global public health problem that affects developing and underdeveloped nations. The most common reason for Fe deficiency is insufficient daily dietary intake. Strategies to combat anemia rely primarily on diet modification to include Fe-rich foods, oral Fe supplementation, or intravenous Fe therapy.[2,6] Fe supplementation strategies carry their own drawbacks due to certain side effects, such as gut inflammation and constipation. In addition, excess Fe promotes the growth of pathogenic bacteria in the gut, which can displace favorable bacterial species and lead to inflammation, endotoxemia, and subsequent diminished nutrient absorption.[7] This cycle of decreased absorption and chronic inflammation associated with anemia contributes to further weakening of the immune system and malnutrition due to ineffective nutrient intake.

While some nutritional minerals are required by the body in large quantities (mg/day), others are necessary in smaller amounts (μg/day) for optimal metabolic function. One such element, selenium (Se), is an essential component of the enzyme glutathione peroxidase, which has important antioxidant functions that protect against cell damage.[2,8,9] Additionally, Se is important for immune health, thyroid hormone metabolism, and proper heart and reproductive functions. Supplementation of Se, especially to younger individuals, is used for addressing this deficiency. However, Se possesses one of the narrowest ranges between effective (< 40 μg/day) and toxic (> 400 μg/day) levels; hence, special care must be taken in Se supplementation to prevent accidental accumulation above the safety threshold.[8] Accordingly, the development of smart and reliable strategies for delivering multiple minerals, with the highest absorption and efficacy along with minimal side effects, would be highly beneficial.

Here, we present micromotors loaded with Fe and Se that are capable of autonomous propulsion in the intestinal fluid, which based on early studies, is expected to enhance localized delivery and absorption of the minerals in the upper intestinal tract to provide anemia relief in an Fe-deficient anemia mouse model. Synthetic micromotor-based dynamic delivery systems have proven to be attractive candidates for the targeted delivery of therapeutic cargoes both in vitro and in vivo.[10–25] Motors with such small dimensions (~5–25 μm), based on different self-propulsion strategies, have been shown to move in different biological fluids while performing a variety of tasks. Micromotors utilized for in vivo gastrointestinal (GI) delivery tasks commonly adopt a core-shell structure with a reactive metal core (magnesium (Mg) or zinc) and an inert shell (titanium dioxide (TiO_2), gold, or various polymers), along with a small opening on one side to enable exposure of the core to the biological fuel.[21,26,27] Due to their material composition, these micromotors are biocompatible and in some cases completely biodegradable.[27] The reaction of the reactive core with GI fluids results in rapid release of hydrogen bubbles from the open end of the micromotor, thus inducing effective motor movement through a bubble thrust.[25] Our early studies demonstrated that the active and autonomous propulsion of these micromotors enables them to embed within the mucosal linings of GI tissues, increasing their residence time and enhancing the absorption and retention of their therapeutic payloads.[17,18,28] With increased absorption, the drug loading can be lowered to achieve the same therapeutic effect while simultaneously reducing adverse side effects. Recently, drug-loaded active micromotors have been incorporated into orally-ingestible tablets, based on common pharmaceutical formulations, in order to localize delivery to the stomach of mice while facilitating convenient administration.[29] Overall, micromotors represent attractive candidates for the targeted and localized delivery of therapeutic cargoes to the GI system.

To address the challenge of relieving anemia and enhancing nutrient adsorption, mineral-loaded micromotors were constructed with a Mg core and a thin TiO_2 shell. The mineral pair of Fe and Se was selected here as a model mineral payload while considering also the potential synergistic effect that Se could have on Fe absorption.[30,31]Additionally, as the key component of the micromotor engine, elemental Mg released as a byproduct of the propulsion reaction could offer additional nutritional benefits in reducing the effects of anemia.[32–34] The Fe and Se minerals were loaded into a chitosan layer and subsequently protected by an enteric pH-responsive polymer to prevent undesired mineral release in the stomach. The Fe/Se loading ratios were optimized to conform with recommended daily dosages while remaining below toxic levels. The movement of the mineral-loaded micromotors was characterized and compared to that of non-loaded motors, demonstrating similar propulsion behavior. Micromotors were administered to anemic mice and various parameters were compared to those of healthy mice and anemic mice treated with control formulations. Hematology data showed significantly higher recovery of important parameters, compared to passive diffusion-based control approaches (*e.g.* red blood cell (RBC) count: $6.9 \times 10^6 \pm 0.6 \times 10^6$ cells/mm^3 *vs.* $4.8 \times 10^6 \pm 0.3 \times 10^6$ cells/mm^3), as will be discussed below. Additionally, blood concentrations of Fe and Se demonstrated improved recovery compared to anemic control groups, while blood and organ analyses revealed no toxicity after 30 days of treatment. These in vivo results indicate that micromotors are

attractive vehicles for the active targeted delivery of mineral supplements, particularly for addressing anemia.

Macronutrients and micronutrients are commonly absorbed in different parts of the GI tract, and it was thus imperative that our supplementation strategy accurately target the correct region (Figure 1a). Our mineral-loaded micromotors were designed to be protected from the highly acidic stomach gastric fluid by an outer pH-responsive enteric coating, Eudragit® L100–55, which is soluble only when pH ≥ 5.5. Upon entering the upper intestinal tract (duodenum), where the pH is ~6, the protective coating can dissolve, thereby exposing the Mg core of the micromotors to the chloride-containing aqueous media and initiating the hydrogen-based propulsion. This protection is crucial to allow micromotors to selectively react and release the cargo in the GI tract but not in the stomach. Our previous studies have demonstrated that the micromotor propulsion causes the motors to impinge on the mucosal layer of the duodenum, increasing retention times compared to inert particles that passively travel through the GI. [17,25] Due to this improved contact with the intestinal wall, the loaded minerals can be more readily absorbed. The Fe and Se minerals, in the forms of iron(II) gluconate hydrate and sodium selenate decahydrate, respectively, were loaded into a positively-charged chitosan layer, which also aids in adhesion to the mucosal layer through electrostatic forces (Figure 1b,c).[35] Iron(II) gluconate is an iron source salt commonly used in many iron supplementation formulations due to its favorable bodily tolerance.[36] Sodium selenate decahydrate has been one of the most common sources of nutritional selenium owing to its high solubility and high bioavailability.[37]

The fabrication of the Fe and Se-loaded micromotors is summarized in Figure 2a (see Methods section). Firstly, Mg microparticles (~20–25 μm) were spread onto a glass slide. Then, a thin, conformal TiO_2 layer was deposited over the Mg microparticles via atomic layer deposition, leaving a small opening where the particle contacts the glass surface. This asymmetry facilitates directional hydrogen bubble generation upon biofluid contact, which generates propulsion thrust. Next, the micromotors were coated with a layer of poly lactide-*co*-glycolic acid (PLGA) to protect them from the more acidic chitosan mineral loading solution which could prematurely activate the motors. Subsequently, the chitosan layer (containing the Fe and Se minerals mixed in at the appropriate ratio) was deposited onto the PLGA layer. Finally, the micromotors were released from the glass slide and were fully coated with an enteric coating (Figure S1).

To confirm the presence of the minerals in the chitosan layer, we performed independent loading of the Fe or Se minerals onto the micromotors (Figure 2b). To facilitate the visualization, the chitosan layers were imaged by introducing fluorescein (FITC) or Rhodamine-6G (Rh-6G) fluorescent dyes with the Fe or Se-loaded micromotors, respectively. Scanning electron microscopy (SEM) and energy-dispersive X-ray spectroscopy (EDX) characterization were performed to confirm the structure of the micromotors and simultaneous mineral loading (Figure 2c). This analysis demonstrated the presence of the Mg core (in blue), the TiO_2 shell with its characteristic opening (in yellow), and the uniform distribution of Fe and Se on the micromotor surface (in green and red, respectively). Next, we tested the propulsion capabilities of the non-loaded Mg/TiO_2/PLGA/chitosan and the Mg/TiO_2/PLGA/Fe-Se@chitosan micromotors in vitro using simulated

intestinal fluid (Figure 2d, Video S1). An efficient propulsion was obtained with both micromotors in chloride-rich intestinal fluid, with the majority of the micromotors propelling for ~3–4 minutes. Compared to the non-loaded motors (mean speed, 164 μm/s), there was a significant decrease in the speed of the nutritional motors (mean speed, 119 μm/s) in simulated intestinal fluid (Figure 2e). However, such speed decrease did not compromise the efficient propulsion of the Fe/Se-loaded micromotors in the tested fluid. After qualitatively evaluating the Fe and Se loading onto the motors, we proceeded to quantitatively measure the amount of each element, along with Mg, that could be delivered per a given dose of micromotors (2 mg of Fe/Se-loaded micromotors) using inductively-coupled plasma/optical-emission spectroscopy (ICP-OES) (Figure 2f–h). For loading, iron(II) gluconate hydrate and sodium selenate decahydrate were dissolved and mixed in a chitosan solution in ratios of 100:50, 100:10, 100:1 and 100:0, keeping the Fe amount constant while varying the Se content. The Fe level increased with lower ratios of added Se, while increased Se levels were observed as we mixed more selenate decahydrate into the chitosan layer (Figure 2f, g). We aimed to optimize the formulation to fit within the daily recommended intake for both minerals (indicated by a purple window) while still staying below the daily toxic upper limit (indicated by a gold line). These ranges and limits were calculated based on the National Institutes of Health (NIH) human dietary references converted for mice (Table S1). Based on these results, we selected the 100:1 ratio and used this formulation for all subsequent in vivo studies. Due to the material composition of our system, the motor core releases Mg ions (as a result of the propulsion reaction), which can be absorbed and used as an additional nutritional supplement (Fig 2h). As Mg is a crucial macronutrient with roles in electrolyte balance and the function of many enzymes, animals require it daily in large amounts.[38] The amount of Mg in the micromotors was determined to be less than daily recommended amount of Mg, most of which can be easily acquired through water consumption.

To assess the therapeutic capabilities of our micromotor system against Fe-deficient anemia, we first induced anemia by feeding young healthy mice with an Fe and Se-deficient diet for 30 days (Figure 3a, red line). The anemia was confirmed by measuring hematology parameters. On the last day of the anemia induction, the RBC, hemoglobin (HGB), and hematocrit (HCT) levels dropped to 5.1×10^6 cells/mm^3, 9.2 g/dL, and 25.0%, respectively, all of which were far below the normal level for male CD1 mice (RBC: $8.5–10.4 \times 10^6$ cells/mm^3, HGB: 13.8–6.8 g/dL, and HCT: 39.3–47.0%).[39] Following induction, anemic mice were orally administered with 30 mg/kg Fe/Se-loaded micromotors per mouse weight every other day for 30 days (Figure 3a, green line and green arrows). Whole blood was collected and the mouse weight was recorded every 6 days after starting the treatment process for 30 days (Figure 3a, green line, blue arrows). Based on the results obtained from our early studies using similar Mg-based micromotors for intestinal delivery,[17,25] we hypothesized here that the formulation's propulsion and ability to embed on the mucosal layer of the intestine, as well as its targeting characteristics (duodenum activation compared to stomach activation), would provide the most efficient mineral absorption. To test this hypothesis, anemic mice were fed with PBS, aqueous extracts of Fe/Se-loaded micromotors (free ion), Fe/Se-loaded micromotors without enteric coating (unprotected motor), and

passive microparticles with enteric coating (passive particle; Figure S2) as controls (see Table S2).

First, we examined the appearance of the ears and feet of the mice at the end of the treatment. The skin tone of the anemic mice treated with Fe/Se-loaded micromotors was rosy and comparable with that of the healthy mice (Figure 3b). In contrast, the mice treated with the free ions, unprotected micromotors, and passive particles all displayed pale skin color, similar to the PBS-treated anemic mice. Moreover, the average body weight of the Fe/Se-loaded micromotors-treated mice was close to that of the healthy mice (Figure S3). Together, these results suggested alleviation of anemia symptoms after treatment with the Fe/Se-loaded micromotor formulation. Anemia is often associated with severe splenomegaly, which is a sign of hypersplenism resulting from a reduction in circulating RBCs.[40] The spleens collected from the Fe/Se-loaded micromotor, free ion, unprotected micromotor, and passive particle-treated groups all showed relieved splenomegaly (Figure 3c). Based on the weight of the spleen compared to body weight, the mice treated with Fe/Se-loaded micromotors (0.37 ± 0.05%) were statistically indistinguishable compared to the healthy mice (0.32 ± 0.06%), which was significantly less than that of the PBS-treated anemic mice (0.87 ± 0.16%). This suggested that the successful delivery of Fe and Se by the Fe/Se-loaded micromotor was able to lessen the hypersplenism by facilitating hematopoiesis.

Next, we proceeded to analyze the biological impact of micromotor-based delivery on representative hematology parameters of the mice (i.e. RBC count, HGB level, and HCT). During the entire treatment period, the PBS-treated group displayed a gradual decrease in these three parameters, indicating the rapid progress of anemia in the absence Fe supplementation (Figure 3d–f). Meanwhile, the free ion, unprotected motor, and passive particle treatments were able to prevent the downward trend in RBC counts, HGB levels, and HCT. However, only the mice administered with the Fe/Se-loaded micromotor exhibited an increase in all of the parameters over time, all of which gradually approached healthy levels. Following treatment, the RBC count of the Fe/Se-loaded micromotor-treated mice was $6.9 \times 10^6 \pm 0.6 \times 10^6$ cells/mm^3, which was near identical to that of the healthy mice ($7.6 \times 10^6 \pm 0.4 \times 10^6$ cells/mm^3) (Figure 3g). Importantly, the RBC count of the Fe/Se-loaded micromotor group was significantly higher than the free ion ($5.5 \times 10^6 \pm 0.8 \times 10^6$ cells/mm^3), unprotected motor ($5.1 \times 10^6 \pm 0.7 \times 10^6$ cells/mm^3), passive particle ($4.8 \times 10^6 \pm 0.3 \times 10^6$ cells/mm^3), and PBS ($2.4 \times 10^6 \pm 0.4 \times 10^6$ cells/mm^3) groups. Similarly, the HGB level of the Fe/Se-loaded micromotor-treated group increased to 11.9 ± 0.8 g/dL and displayed significant improvement when compared with the free ion (9.4 ± 1.0 g/dL), non-loaded motors (8.5 ± 1.0 g/dL), passive particles (8.9 ± 0.6 g/dL), and PBS (3.5 ± 0.4 g/dL) groups (Figure 3h). In terms of the HCT, the Fe/Se-loaded micromotor treatment successfully boosted the value to 31.5 ± 2.8% while that of healthy mice remained at 40.2 ± 1.8%. The HCT in the free ion (24.3 ± 2.3%), unprotected motor (21.7 ± 1.8%), passive particle (22.2 ± 2.0%), and PBS (8.3 ± 1.1%) groups were significantly lower than that of the healthy mice (Figure 3i). Overall, one possible explanation to the lower HCT values of the free ion, unprotected micromotor and non-propelled particle groups, is their short residence in the duodenum due to a lack of propulsion or premature activation in the stomach. In contrast, Fe/Se-loaded micromotor treatment outperformed the rest of the

treatment controls and ameliorated anemia symptoms by boosting RBC counts, HGB, and HCT levels.

To gain insight into the effect of the various treatments on mineral levels, we analyzed the elemental Fe and Se content of whole blood at the experiment's endpoint via inductively-coupled plasma mass spectroscopy (ICP-MS) (Figure 3j, k). After Fe/Se-loaded micromotor motor treatment, the ^{56}Fe content in the blood increased to 391 ± 23 μg/g, which was significantly higher than the other control groups, including the free ion (183 ± 16 μg/g), unprotected motor (178 ± 12 μg/g), passive particle (196 ± 24 μg/g), and PBS (145 ± 18 μg/g) groups (Figure 3j). Similarly, the ^{78}Se content from the Fe/Se-loaded micromotor treatment group (0.21 ± 0.024 μg/g) was higher compared to the other groups (Figure 3k; free ions: 0.13 ± 0.040 μg/g, unprotected motors: 0.13 ± 0.031 μg/g, passive particles: 0.15 ± 0.011 μg/g, and PBS: 0.13 ± 0.017 μg/g). These mineral level quantifications suggest that actively propelled micromotor is capable for delivering both Fe and Se to the circulation system, which leads to a noticeable relief of anemia.

Lastly, we sought to evaluate the toxicity of the Fe/Se-loaded micromotor following the treatment regimen. A treatment dosage of 30 mg/kg of Fe/Se-loaded was orally administered to mice every other day for 30 days, while non-treated mice served as controls. At the end of the study, we performed a comprehensive chemistry analysis of the blood and quantified major blood cell populations (Figure 4a,b). No statistical difference was observed between the control group and the Fe/Se-loaded micromotor treatment group in any of the blood composition and blood cell parameters that were studied. Next, we evaluated the toxicity of the Fe/Se-loaded micromotor to the GI tract and major organs by carefully examining tissue histology. The stomach and lower GI tract from the Fe/Se-loaded micromotor-treated group exhibit undamaged mucosa, submucosa, and muscle structures (Figure 4c). No lymphocyte infiltration to the mucosal layer was observed, indicating the absence of inflammation. The appearance of other major organs (kidneys, spleen, lungs, liver, and heart) was normal and similar to that of the healthy mice Figure 4d. Together, these results suggested that the Fe/Se-loaded micromotor represents a safe platform for oral application.

Despite modern food growing technology and global food trade routes, a large fraction of the population still suffers from major nutritional deficiencies. New highly efficient strategies for delivering multiple minerals are thus critically desired. With this in mind, we have developed an autonomous, dynamic micromotor-based delivery platform toward active supplementation of Fe and Se. This active delivery platform was tested in a mouse model of anemia and compared to passive and non-targeted controls, as well as free dissolved minerals. The dynamic mineral-loaded micromotor group outperformed the different control treatments, leading to significant recovery of important hematological parameters, such as RBC counts, HGB, and HCT levels, as well as blood Fe and Se levels. At the same time, our active delivery system showed no local or systemic toxicity after a 30-day treatment.

These encouraging results highlight the advantages of using a self-propelled active micromotor delivery platform to enhance the mineral absorption efficacy and relieve Fe-deficient anemia. Another excellent feature of this system is its versatility. While we delivered Fe and Se minerals in the present work, a variety of other inorganic salts and

vitamins could be readily loaded, depending on the specific demand. Importantly, by providing more efficient mineral absorption, this active delivery strategy facilitates dose sparing, which can have the added benefit of reducing potential side effects. While in this study we chose a strategy previously shown to provide targeting of the duodenum - for optimal nutrient absorption, delivery to other parts of the GI tract could be also achieved by tailoring the thickness of the enteric coating.[17] Targeting of the stomach could also be realized by substituting the present enteric coating with an acid-labile alternative. Additionally, we have shown recently that micromotors can be loaded into pill formulations for more concentrated release and localization in the body, bringing this delivery platform closer to translation to practical applications. Such pill formulation will make the active delivery of nutrients more economical, analogous to existing supplements. Finally, our system is biocompatible, highly biodegradable, and non-toxic. By optimizing material composition and layer thickness, we can program the disintegration of the micromotor to control subsequent absorption and biodegradation. The micromotors have certain limitations as well. For example, despite the fact that one fabrication batch can produce thousands of micromotors, scalability could remain a bottleneck due to the number of sequential layers involved in the fabrication. At the same time, the materials and equipment used is common to most laboratories with the exception of the atomic layer deposition technique. Thus, it should be feasible to eventually translate micromotor fabrication to industrial scales although the costs would most likely be higher compared to common pill fabrication techniques. Looking forward, the impact of micromotor-based delivery on a more comprehensive set of biomarkers, including those specific to the metabolism of individual nutrients, will need to be studied in further detail. Considering the encouraging results of this study, yet keeping in mind the challenges of clinical adoption, further improvements of our dynamic delivery platform are desired towards precise navigation and localization inside the body, along with exhaustive in-vivo biocompatibility studies, elimination of micromotor residues using fully transient materials, and even higher efficiency. Ultimately, this proof-of-concept work demonstrating the utility of efficient motor-based nutrition supplementation could pave the way for similar approaches with clinical applicability.

Methods

Micromotor fabrication.

The Mg-based micromotors were prepared using commercially available magnesium microparticles (catalog #FMW20, TangShan WeiHao Magnesium Powder Co.; average size, 20 ± 5 μm) as the core. The Mg microparticles were initially washed with acetone to eliminate impurities. After drying under a N_2 current, the Mg microparticles were dispersed onto glass slides (10 mg of Mg microparticles per glass slide) and coated with TiO_2 by atomic layer deposition at 100 °C for 3000 cycles using a Beneq TFS 200 system. Being a chemical vapor deposition technique, the process utilizes gas phase reactants, leading to uniform coatings over the Mg microparticles, while leaving a small opening (~2 μm) at the contact point of the microparticle to the glass slide. The Mg/TiO_2 micromotors were coated with 120 μL of 1% (w/v) PLGA (Sigma-Aldrich, P2191) prepared in ethyl acetate (Sigma-Aldrich, 270989); this process was repeated to ensure the protection of the Mg-based motors from reaction with the chitosan solution during the mineral loading step. Then, iron(II)

gluconate hydrate (100 mg/mL; Sigma-Aldrich, 44948) and sodium selenate decahydrate (1 mg/mL; Alfa Aesar, AA1423914) were dissolved in a 0.05% (w/v) chitosan solution (Sigma-Aldrich, C3646) and prepared in water containing 0.01% (w/v) sodium dodecyl sulfate (Sigma-Aldrich, C436143) and 3 mM acetic acid (Sigma-Aldrich, 695092). The Mg/TiO_2-PLGA micromotors were coated with 100 μL of this solution and dried under a N_2 current. Finally, the mineral-loaded micromotors were collected by lightly scratching the microparticles off the glass slide. It is important to mention that in order to achieve dose equivalence between the treatment and control groups, we first fabricated a large batch of Fe/Se-loaded micromotors. After the fabrication, a fraction of the resulting micromotors was separated and protected with the enteric coating and used as the treatment group. Another fraction of the micromotors was left uncoated and used as the unprotected micromotor control group. The third fraction of micromotors was dissolved and the extract was used as the free ion control. To compare with the Mg-based micromotors, inert 20 μm silica microparticles (Nanocs, Inc., Si01–20u-1) were used as core particles (Supporting Figure S2), following the same protocol described above, and used as the passive particle control. Such inert silica microparticles do not react with intestinal fluid and thus do not exhibit propulsion.

Micromotor enteric coating.

The commercial enteric polymer Eudragit L100–55 (Evonik Industries) was chosen to coat the mineral-loaded micromotors to prevent the Mg core from reacting in the gastric fluid of the stomach. To start, a batch of mineral-loaded micromotors was added in 100 μL of a 6.5% (w/v) Eudragit L100–55 solution prepared in pure isopropyl alcohol. The micromotor suspension was then dispersed into a paraffin oil (Sigma-Aldrich, 18512) and Span 85 (Sigma-Aldrich, S7135) matrix (100:1 ratio) and left under continuous stirring for 2 h. Then, 1 mL of hexanes (Sigma-Aldrich, 296090) was added following an overnight solvent evaporation process. The enteric coating was further hardened by the introduction of fresh hexanes, followed by a subsequent period of soft annealing at 70 °C for 2 h, which ensured complete sealing of the mineral-loaded motors. The passive control microparticles were fabricated following a similar process.

Micromotor characterization.

SEM imaging of a mineral-loaded micromotor was obtained with an FEI Quanta 250 ESEM instrument, using an acceleration voltage of 10 kV. EDX mapping analysis was performed using an Oxford EDX detector attached to the SEM instrument and operated by Pathfinder software. For additional characterization, iron(II) gluconate hydrate or sodium selenate decahydrate were loaded in chitosan layers further labeled with FITC (λ_{ex}=492 nm/ λ_{em}=520 nm, Sigma-Aldrich, 46945) or Rh-6G (λ_{ex}=524 nm/ λ_{em}=547 nm, Sigma-Aldrich, R4127) fluorescent dyes, respectively. Brightfield and fluorescent images of the mineral-loaded motors were captured using an Invitrogen EVOS FL microscope coupled with a 10× and 40× microscope objectives using the GFP and RFP fluorescence filters for green and red excitation, respectively.

Micromotor propulsion.

The autonomous propulsion of the mineral-loaded micromotors was tested in vitro using a simulated intestinal fluid (Sigma-Aldrich, 53757). The intestinal fluid was diluted 10 times according to the manufacturer's specifications (final pH ~6.5) and supplemented with 0.2% Triton X-100 (Fisher Scientific, 9002-93-1) as a surfactant. An inverted optical microscope (Nikon Eclipse Ti-S/L100) coupled with different microscope objectives (10×, 20×, and 40×) along with a Hamamatsu C11440 digital camera and NIS Elements AR 3.2 software were used to capture the videos. The speed of the micromotors was tracked using an NIS Elements tracking module.

Mineral quantification by ICP-OES.

Mineral levels for Fe, Se, and Mg were obtained using a PerkinElmer Optima 3000 DV system with a plasma power of 1450 W and sensitivity calibration with 1 ppm manganese. The elements were measured at the following wavelengths: 238.2, 196.0, 285.2 nm for Fe, Se, and Mg, respectively. Samples from different Fe/Se loading ratios (100:50, 100:10, 100:1, and 100:0) were prepared and measured by modifying an existing protocol.[27] In short, 2 mg dosages of non-loaded and loaded micromotors were put in conical tubes followed by dissolution in 5 mL of 0.1 M hydrochloric acid (EMD Millipore, HX0603–4) overnight. Then the samples were spun down at 4000 RPM for 15 min on an IEC CL31R Multispeed centrifuge (Thermo Scientific) to ensure no solid particles were introduced into the plasma. The supernatant was further diluted 20× with 1% trace metal-grade nitric acid (HNO_3) (Fischer Chemical, A509-P500). Finally, a concentration calibration for Fe, Se, and Mg was performed with commercial multielement standards prior to analysis (SPEX CertiPrep, MIXSTD1–100, and MIXSTD5A-100).

Animal care.

Mice were housed in an animal facility at UC San Diego in compliance with local, state, federal, and National Institutes of Health guidelines. All of the animal experiments were performed according to protocols that were previously reviewed and approved by the Institutional Animal Care and Use Committee at UC San Diego.

Generation of Fe/Se-deficient mouse model.

A month prior to treatment, 3-week-old male CD1 mice (n = 30) were obtained from Charles River Laboratories (Wilmington, MA). To induce the Fe and Se deficiency, 25 mice were fed with a deficient diet (Se < 0.01 ppm, Fe < 6 ppm, Teklad Custom Diet, TD.80396, Envigo). Every week, 250 μL of blood was drawn to accelerate the Fe and Se depletion. In the control group, 5 mice were fed with the standard chow (~270 ppm Fe). To confirm the Fe and Se deficiency, 100 μL of blood was collected into heparin-pretreated tubes (5 μL, 10 mg/mL, Sigma-Aldrich) at day 30 to quantify the Fe and Se content with ICP-MS. Meanwhile, the Fe deficiency-induced anemia was evaluated by measuring the hematological parameters from the whole blood with a scil Vet abc Plus™ machine (scil Animal Care Company). Parameters including RBC counts, HGB concentration, and HCT were recorded to reflect the severity of anemia.

In vivo Fe and Se replenishment with mineral-loaded micromotors.

Fe/Se-deficient mice were randomly divided into 5 groups (n = 5) at the beginning of the treatment. The phenotype was evaluated by a researcher who was not informed of the treatment groups. The dosing scheme was as follows: 30 mg/kg Fe/Se-loaded micromotor, free ion, unprotected micromotor, and passive particle formulations were orally administered to the deficient mice every other day for 30 days. In order to ensure the amount of free ions was equivalent to the ions loaded onto the micromotors, we allocated the same amount of micromotors used in the treatment group (2 mg) and then dissolved them in diluted HCl and spun down to remove undesired solid debris. Subsequently, the extracted liquid was orally administered to the mice. The healthy mice in the control group were left untreated. Every 6 days, 100 μL of blood from each mouse was sampled to monitor the RBC counts, HGB levels, and HCT. At the end of the treatment, 300 μL of blood was withdrawn from each mouse and Fe and Se were quantified by ICP-MS. Statistical analysis was performed using one-way ANOVA. The study was repeated twice demonstrating reproducibility between the two trials.

Mineral quantification of mouse blood by ICP-MS.

ICP-MS mineral level analysis of mouse blood was performed on a Thermo Scientific iCAP RQ ICP-MS operating in Kinetic Energy Discrimination mode. We used an RF plasma power of 1550 W with a quartz cyclonic spray chamber, Ni cone, a dwell time of 0.04 s, and 20 replicates per each sample. The sample preparation was modified from existing protocols.[41–43] In short, blood with known mass was placed in a vial. Then, ~5 mL of 70% trace metal grade HNO_3 was added to the vial and left overnight on a hotplate at 100 °C. The next day, the samples were dried by uncapping them and leaving them on the hot plate. Another ~5 mL of 70% trace metal grade HNO_3 was added to redisperse the yellow/brown residue and the samples were left overnight again at 100 °C. The next day, 2 mL of 30% H_2O_2 (Fischer Chemical, H325–500) was added to decompose leftover organic species and the samples were left at 120 °C overnight. This step was repeated 2 more times. Finally, the samples were dried on the hotplate and redispersed in 10 mL of 1% trace metal grade HNO_3. Then, samples were further diluted in order to prevent ICP-MS detector saturation and spiked with an internal indium standard (Inorganic Ventures, Virginia, USA, IV-ICPMS-71D). Finally, a concentration calibration for ^{56}Fe and ^{78}Se isotopes was performed with commercial multielement standard prior to analysis (Inorganic Ventures, Virginia, USA, IV-ICPMS-71A). These isotopes were chosen as the most stable and prevalent isotopes for these elements.

Toxicity evaluation of mineral-loaded micromotors.

Seven-week-old male CD1 mice were purchased from Charles River Laboratories. Mice were randomly divided into two groups. One group of mice was orally administrated with 30 mg/kg of the Fe/Se-loaded micromotors, while the other group was dosed with 200 μL of deionized water (n = 3). The dosing frequency was kept the same as the treatment study (every other day for 30 days). At the end of the study, mice were fasted for 12 h before sample collection. For the blood cell count, 100 μL of blood was withdrawn into EDTA-pretreated tubes (Sarstedt). The white blood cell, RBC, and platelet counts were recorded

with a scil Vet abc Plus™ machine. For the comprehensive metabolic panel, 300 μL of blood was collected into heparin-pretreated tube. Serum was separated by centrifuging the blood at 1000 *g* for 5 min. The serum samples were then submitted to the UC San Diego Animal Care Program Diagnostic Services Laboratory for analysis. To evaluate the toxicity of the micromotors to major organs, mice were euthanized and perfused with 30 mL of PBS. The heart, liver, kidney, spleen, and lung were then collected. The stomach was removed from abdominal cavity and cut open along the large curvature. The food was removed, and the tissue was rinsed in PBS. The remaining GI tract was cut into 4 sections: the colon, proximal small intestine, middle small intestine, and distal small intestine. The small intestine sections were of equal length. The samples were prepared following a previously published swiss-rolling protocol.[44] In brief, the intestine segments were gently flushed with PBS to fully remove their contents. The gut segment was then cut open longitudinally along the mesenteric line and placed in clean petri dish with the luminal side facing upwards. A clean toothpick was used to wrap the intestine segments, and the rolls were transferred to tissue-embedding cassettes. All of the organs were fixed, dehydrated, and sectioned for H&E staining. Images were taken by a Nanozoomer 2.0-HT slide scanning system.

Supplementary Material

Refer to Web version on PubMed Central for supplementary material.

ACKNOWLEDGMENT

This work was supported by the Defense Threat Reduction Agency Joint Science and Technology Office for Chemical and Biological Defense (Grant Numbers HDTRA1-14-1-0064 and HDTRA1-13-1-0002), and the National Institutes of Health under Award Number R01CA200574. E.K. acknowledges the Charles Lee Powell Foundation and for financial support. R. M-U. acknowledges the support from the Fulbright grants and the Conicyt PFCHA/Doctorado becas Chile/2015–56150011. M.B.-G. acknowledges a postdoctoral fellowship from Consejo Nacional de Ciencia y Tecnología (CONACyT).

We thank Prof. Paterno Castillo and Chris MacIsaac for help with the ICP-OES measurements. We thank Dr. Neal Arakawa for assistance with the ICP-MS experiments.

REFERENCES

(1). Gupta UC; Gupta SC Sources and Deficiency Diseases of Mineral Nutrition in Human Health and Nutrition: A Review. Pedosphere 2014, 24, 13–38.

(2). Soetan KO; Olaiya CO; Oyewole OE The Importance of Mineral Elements for Humans, Domestic Animals and Plants: A Review. Afr. J. Food Sci 2010, 4, 200–222.

(3). Van Wayenburg CAM; van de Laar FA; van Weel C; van Staveren WA; van Binsbergen JJ Nutritional Deficiencies In General Practice: A Systematic Review. Eur. J. Clin. Nutr 2005, 59, 81–88.

(4). Zimmermann MB; Hurrell RF Nutritional Iron Deficiency. Lancet 2007, 370, 511–520. [PubMed: 17693180]

(5). Camashella C Iron-Deficiency Anemia. N. Engl. J. Med 2015, 372, 1832–1843. [PubMed: 25946282]

(6). Armstrong GR The Lucky Iron Fish: A Simple Solution For Iron Deficiency. Blood Adv. 2017, 1, 330. [PubMed: 29296948]

(7). Stelle I; Kalea AZ; Pereira DIA Iron Deficiency Anaemia: Experiences And Challenges. Proc. Nutr. Soc 2019, 78, 19–26. [PubMed: 29986781]

(8). Fordyce FM Selenium Deficiency and Toxicity in the Environment In Essentials of Medical Geology; Selinus O, Ed.; Springer: New York, 2013; pp 375–416.

(9). Cueto S Breakfast and Performance. Public Health Nutr 2001, 4, 1429–1431. [PubMed: 11918495]

(10). Jang D; Jeong J; Song H; Shung SK Targeted Drug Delivery Technology Using Untethered Microrobots: A Review. J. Micromech. Microeng 2019, 29, 053002.

(11). Abdelmohsen LKEA; Peng F; Tu Y; Wilson DA Micro- and Nano-Motors for Biomedical Applications. J. Mater. Chem. B 2014, 2, 2395–2408.

(12). Esteban-Fernández de Ávila B; Gao W; Karshalev E; Zhang L; Wang J Cell-Like Micromotors. Acc. Chem. Res 2018, 51, 1901–1910. [PubMed: 30074758]

(13). Wang H; Pumera M Emerging Materials for The Fabrication of Micro/Nanomotors. Nanoscale 2017, 9, 2109–2116. [PubMed: 28144663]

(14). Shao J; Xuan M; Zhang H; Lin X; Wu Z; He Q Chemotaxis-Guided Hybrid Neutrophil Micromotors For Targeted Drug Transport. Angew. Chem 2017, 56, 12935–12939. [PubMed: 28816386]

(15). Karshalev E; Esteban-Fernández de Ávila B; Wang J Micromotors for “Chemistry-On-The-Fly”. J. Am. Chem. Soc 2018, 140, 3810–3820. [PubMed: 29470916]

(16). Fusco S; Sakar MS; Kennedy S; Peters C; Bottani R; Starsich F; Mao A; Sotiriou GA; Pané S; Pratsinis SE; Mooney D; Nelson BJ An Integrated Microrobotic Platform for On-Demand, Targeted Therapeutic Interventions. Adv. Mater 2013, 26, 952–957. [PubMed: 24510666]

(17). Li J; Thamphiwatana S; Liu W; Esteban-Fernández de Ávila B; Angsantikul P; Sandraz E; Wang J; Xu T; Soto F; Ramez V; Wang X; Gao W; Zhang L; Wang J Enteric Micromotor Can Selectively Position and Spontaneously Propel in The Gastrointestinal Tract. ACS Nano 2016, 10, 9536–9542. [PubMed: 27648483]

(18). Esteban-Fernández de Ávila B; Angsantikul P; Li J; Lopez-Ramirez MA; Ramírez-Herrera DE; Thamphiwatana S; Chen C; Delezuk J; Samakapiruk R; Ramez V; Obonyo M; Zhang L; Wang J Micromotor-Enabled Active Drug Delivery For In Vivo Treatment Of Stomach Infection. Nat. Comm 2017, 8, 272.

(19). Wang H; Pumera M Micro/Nanomachines And Living Biosystems: From Simple Interactions to Microcyborgs. Adv. Funct. Mater 2018, 28, 1705421.

(20). Felfoul O; Mohammadi M; Teherkhani S; de Lanauze D; Xu YZ; Loghin D; Essa S; Jancik S; Houle D; Lafleur M; Gaboury L; Tabrizian M; Kaou N; Atkin M; Vuong T; Batist G; Beauchemin N; Radzioch D; Martel S Magneto-Aerotactic Bacteria Deliver Drug-Containing Nanoliposomes To Tumour Hypoxic Regions. Nat. Nanotechnol 2016, 11, 941–947. [PubMed: 27525475]

(21). Li J; Angsantikul P; Liu W; Esteban-Fernández de Ávila B; Thamphiwatana S; Xu M; Sandraz E; Wang X; Delezuk J; Gao W; Zhang L; Wang J Micromotors Spontaneously Neutralize Gastric Acid For Ph-Responsive Payload Release. Angew. Chem. Int. Ed. Engl 2017, 56, 2156–2161. [PubMed: 28105785]

(22). Tu Y; Peng F; White PB; Wilson DA Redox-Sensitive Stomatocyte Nanomotors: Destruction and Drug Release in The Presence of Glutathione. Angew. Chem. In. Ed. Engl 2017, 56, 7620–7624.

(23). Chen C; Chang X; Angsantikul P; Li J; Esteban-Fernández de Ávila B; Karshalev E; Liu W; Mou F; He S; Castillo R; Liang Y; Guan J; Zhang L; Wang J Chemotactic Guidance Of Synthetic Organic/Inorganic Payloads Functionalized Sperm Micromotors. Adv. Biosyst 2017, 2, 1700160.

(24). Hortelão AC; Patiño T; Perez-Jiménez A; Blanco À; Sánchez S Enzyme-Powered Nanorobots Enhance Anticancer Drug Delivery. Adv. Funct. Mater 2018, 28, 1705086.

(25). Esteban-Fernández de Ávila B; Angsantikul P; Li J; Gao W; Zhang L; Wang J Micromotors Go In Vivo: From Test Tubes to Live Animals. Adv. Funct. Mater 2018, 28, 1705640.

(26). Chen C; Karshalev E; Guan J; Wang J Magnesium-Based Micromotors: Water-Powered Propulsion, Multifunctionality, And Biomedical and Environmental Applications. Small 2018, 14, 1704252.

(27). Chen C; Karshalev E; Li J; Soto F; Castillo R; Campos I; Mou F; Guan J; Wang J Transient Micromotors That Disappear When No Longer Needed. ACS Nano 2016, 10, 10389–10396. [PubMed: 27783486]

(28). Gao R; Dong R; Thamphiwatana S; Li J; Gao W; Zhang L; Wang J Artificial Micromotors in The Mouse's Stomach: A Step Towards In Vivo Use of Synthetic Motors. ACS Nano 2015, 9, 117–123. [PubMed: 25549040]

(29). Karshalev E; Esteban-Fernández de Ávila B; Beltrán-Gastélum M; Angsantikul P; Tang S; Mundaca-Uribe R; Zhang F; Zhao J; Zhang L; Wang J Micromotor Pills As A Dynamic Oral Delivery Platform. ACS Nano 2018, 12, 8397–8405. [PubMed: 30059616]

(30). Watts DL The Nutritional Relationships of Iron. J. Orthomol. Med 1988, 3, 110–116.

(31). Semba RD; Ricks MO; Ferrucci L; Xue Q-L; Guralnik JM; Fried LP Low Serum Selenium Is Associated With Anemia Among Older Adults In The United States. Eur. J. Clin. Nutr 2009, 63, 93–99. [PubMed: 17805227]

(32). Ige AO; Adewoye EO Oral Magnesium Treatment Reduces Anemia and Levels of Inflammatory Markers in Experimental Diabetes. J. Diet. Suppl 2016, 14, 76–88. [PubMed: 27459339]

(33). Shi Z; Hu X; He K; Yuan B; Garg M Joint Association of Magnesium and Iron Intake With Anemia Among Chinese Adults. Nutrition 2008, 24, 977–984. [PubMed: 18586459]

(34). De Franceschi L; Brugnara C; Beuzard Y Dietary Magnesium Supplementation Ameliorates Anemia in a Mouse Model Of B-Thalassemia. Blood 1997, 90, 1283–1290. [PubMed: 9242563]

(35). Hejazi R; Amiji M Chitosan-Based Gastrointestinal Delivery Systems. J. Controlled Release 2003, 89, 151–165.

(36). Defence Science and Technology Organisation. Low Dose Ferrous Gluconate Supplement Fails to Alter the Iron Status of Female Officers-in-Training; DSTO-RR-0297; Australian Government Department of Defence: Victoria, Australia, 2005.

(37). Podoll KL; Bernard JB; Ullrey DE; DeBar SE; Ku PK; Magee KT Dietary Selenate Versus Selenite for Cattle, Sheep, And Horses. J. Anim. Sci 1992, 70, 1965–1970. [PubMed: 1321804]

(38). Grzebisz W Magnesium - Food and Human Health. J. Elem 2011, 16, 299–323.

(39). Serfilippi LM; Pallman DR; Russell B Serum Clinical Chemistry and Hematology Reference Values in Outbred Stocks of Albino Mice From Three Commonly Used Vendors and Two Inbred Strains of Albino Mice. Contemp. Top. Lab. Anim. Sci 2003, 42, 46–52.

(40). Motulsky AG; Casserd F; Giblett ER; Broun GO; Finch CA Anemia and The Spleen. N. Engl. J. Med 1958, 259, 1215–1219. [PubMed: 13622913]

(41). Uddin ABMH; Khalid RS; Alaama M; Abdualkader AM; Kasmuri A; Abbas SA Comparative Study of Three Digestion Methods for Elemental Analysis in Traditional Medicine Products Using Atomic Absorption Spectrometry. J. Anal. Sci. Technol 2016, 7, 1–7.

(42). Harrington JM; Young DJ; Essader AS; Sumner SJ; Levine KE Analysis of Human Serum and Whole Blood for Mineral Content By ICP-MS and ICP-OES: Development of A Mineralomics Method. Biol. Trace Elem. Res 2014, 160, 132–142. [PubMed: 24917052]

(43). Enders A; Lehmann J Comparison of Wet-Digestion and Dry-Ashing Methods for Total Elemental Analysis of Biochar. Commun. Soil Sci. Plant Anal 2012, 43, 1042–1052.

(44). Bialkowska AB; Ghaleb AM; Nandan MO; Yang VW Improved Swiss-Rolling Technique for Intestinal Tissue Preparation for Immunohistochemical and Immunofluorescent Analyses. J. Vis. Exp 2016, 113, e54161.

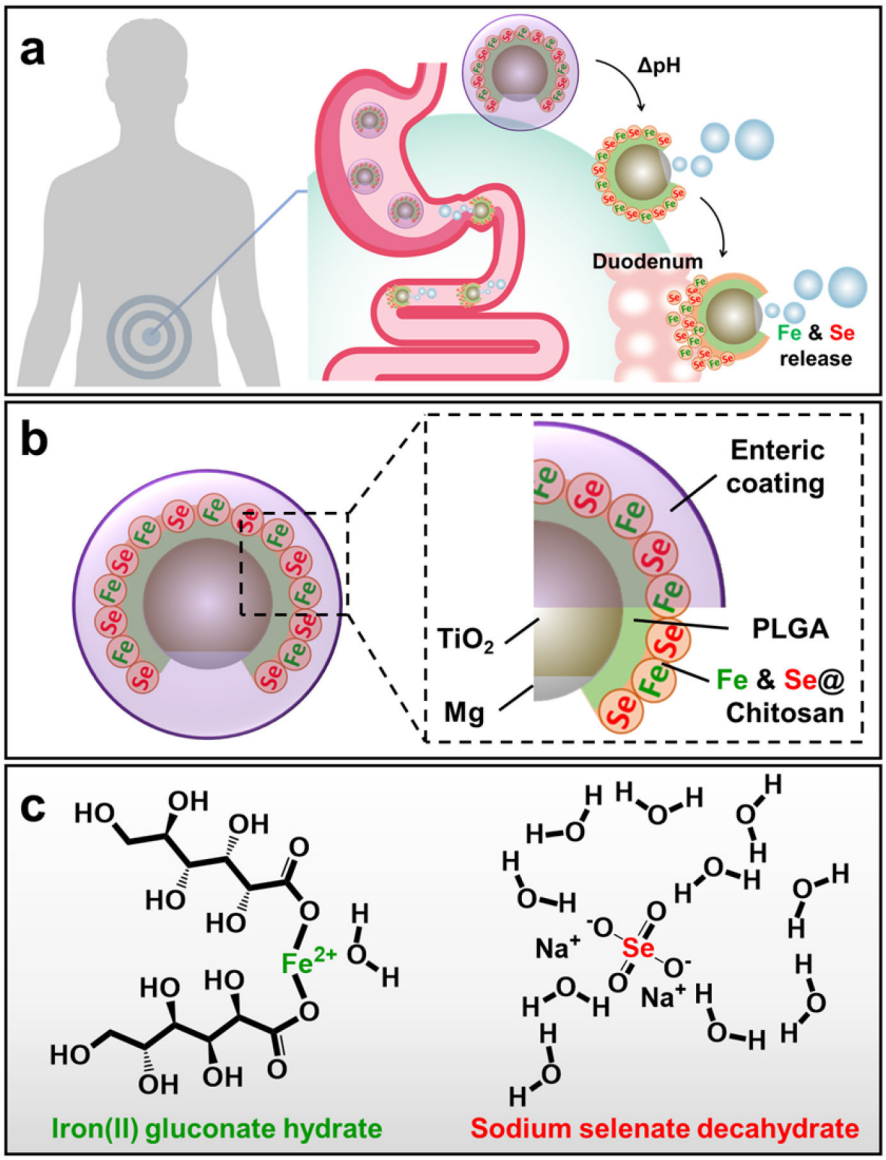

Figure 1.

Schematic illustrations of synthetic micromotors for active delivery of minerals. a, Schematic of micromotor-based in vivo delivery and release of Fe and Se at the duodenum region. b, Schematic structure of the mineral-loaded micromotor consisting of a Mg/TiO2 core protected with an inner PLGA polymer layer, a middle chitosan layer loaded with Fe and Se, and an outer pH-responsive enteric layer (Eudragit® L100–55, soluble when pH ≥ 5.5). c, Chemical structures of iron(II) gluconate hydrate (left) and sodium selenate decahydrate (right).

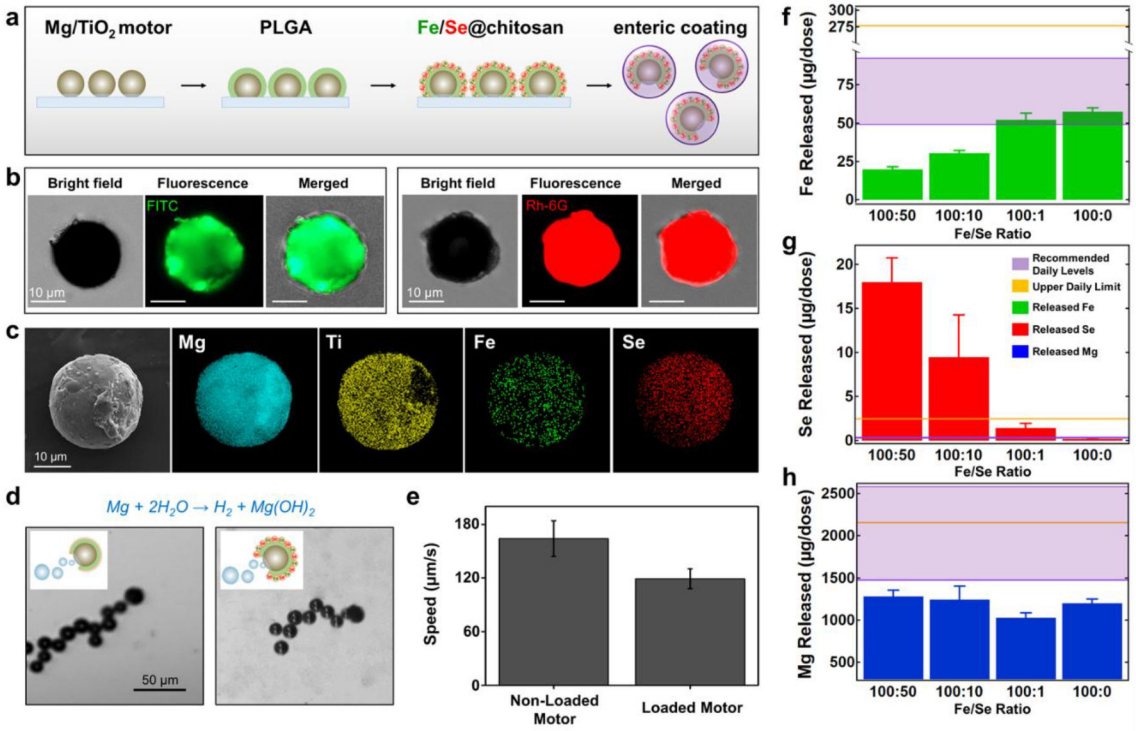

Figure 2.

Micromotor preparation, structural characterization and mineral loading. a, Schematic of the micromotor preparation. TiO_2 is deposited over Mg microparticles dispersed over a glass slide, a PLGA film is coated over the Mg/TiO_2 micromotors, Fe and Se are loaded via a chitosan film, and an enteric layer is coated over the mineral-loaded micromotors with the pH-responsive polymer Eudragit L100–55. b, Demonstration of the Fe and Se loading: iron(II) gluconate hydrate (left) and sodium selenate decahydrate (right) loaded in FITC or Rh-6G-labeled chitosan films, respectively. The microscopy images (optical, fluorescence: GFP and RFP channels, and merged) demonstrate the loading of the Fe and Se-based compounds over the Mg-based micromotors. c, SEM image of a Mg/TiO_2/PLGA/Fe-Se@chitosan micromotor and EDX images illustrating the distribution of elemental Mg (cyan), Ti (yellow), Fe (green), and Se (red). d, Microscopic images (corresponding to Video S1) and schematic insets displaying the hydrogen bubble generation and the motion of a non-loaded (left) and a mineral-loaded (right) micromotor in intestinal fluid simulant (pH ~6.5) supplemented with 0.2% Triton X-100 (used as surfactant). e, Comparison of the non-loaded and mineral-loaded micromotor speeds in simulated intestinal fluid (n = 3, mean ± SD). f-h, Released elemental Fe (f), Se (g), and Mg (h) per treatment dosage (2 mg of Fe/Se-loaded micromotors) as a function of different ratios of the Fe and Se compounds used to prepare mineral-loaded micromotors (n = 4, mean ± SD). Two mg of mineral-loaded micromotors, dissolved in 0.1 M hydrochloric acid solution, were used to perform the ICP-OES analysis. The purple window indicates the recommended daily intake levels, and the gold line indicates the upper daily limit of both elements.

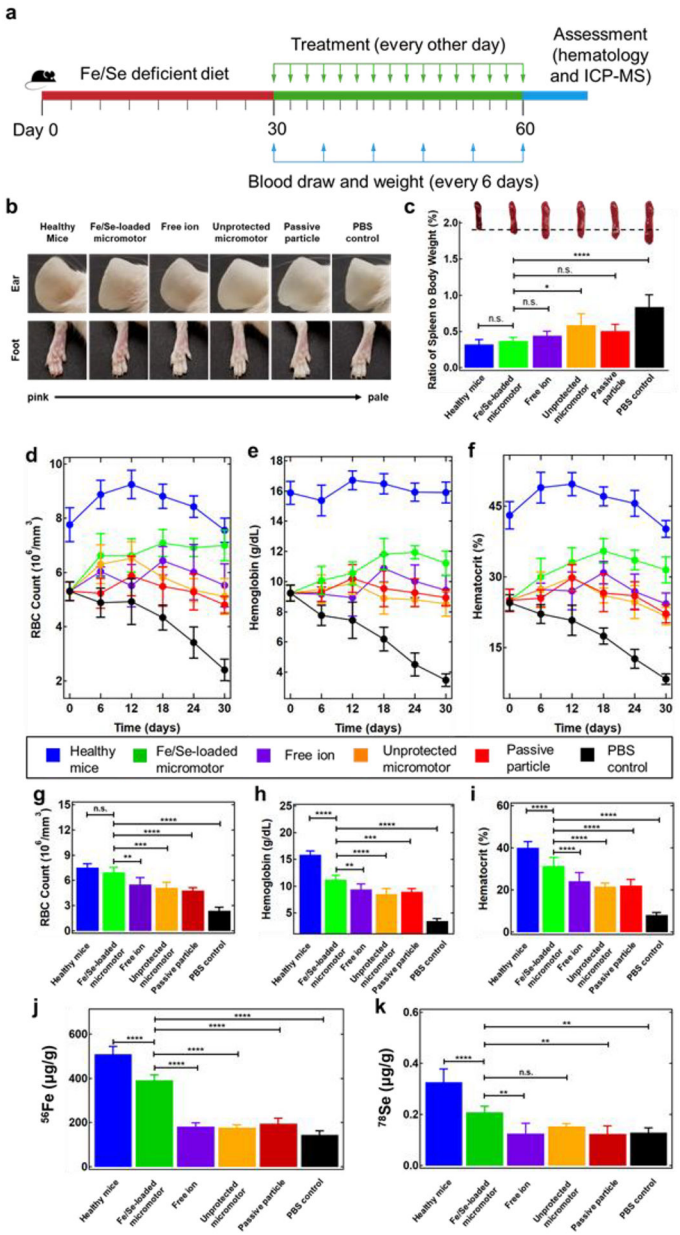

Figure 3.

Active mineral replenishment with Fe/Se-loaded micromotors. a, The study protocol for evaluating treatment efficacy of Fe/Se-loaded micromotors using an anemic mouse model. Anemia was induced by feeding mice with Fe and Se deficient diet for 30 days (red line). Subsequently, the mice treatment was performed for 30 days (green line) with micromotor and control administration every other day (green arrows). Blood draw and weighing of the mice were performed every 6 days during the treatment period (blue arrows). Images of mice, hematology and ICP-MS measurements were carried out at the end of the study (blue line). b, Representative images of mouse ears (top) and feet (bottom) demonstrating differences in coloration and vein visibility among the six tested groups. c, Ratio of spleen weight to total body weight of mice treated with the six tested groups. Inset images show a

representative spleen from each group, highlighting the changes in spleen color and size. d-f, RBC count (10^6 cells/mm^3) (d), hemoglobin levels (g/dL) (e), and hematocrit (%) (f) of each group of mice were measured and monitored for 30 days over the entire treatment period. g-i, RBC (10^6 cells/mm^3) (g), hemoglobin (g/dL) (h) and hematocrit (%) (i) of each group of mice quantified at the endpoint of the treatment (on day 30). j, k Elemental ^{56}Fe (μg/g) (j) and ^{78}Se (μg/g) (k) content of whole blood for each group of mice, quantified by ICP-MS at the endpoint of the treatment (on day 30). Each group had n = 5 mice. Statistical analysis was performed using one-way ANOVA (error bars are defined as mean ± SD).

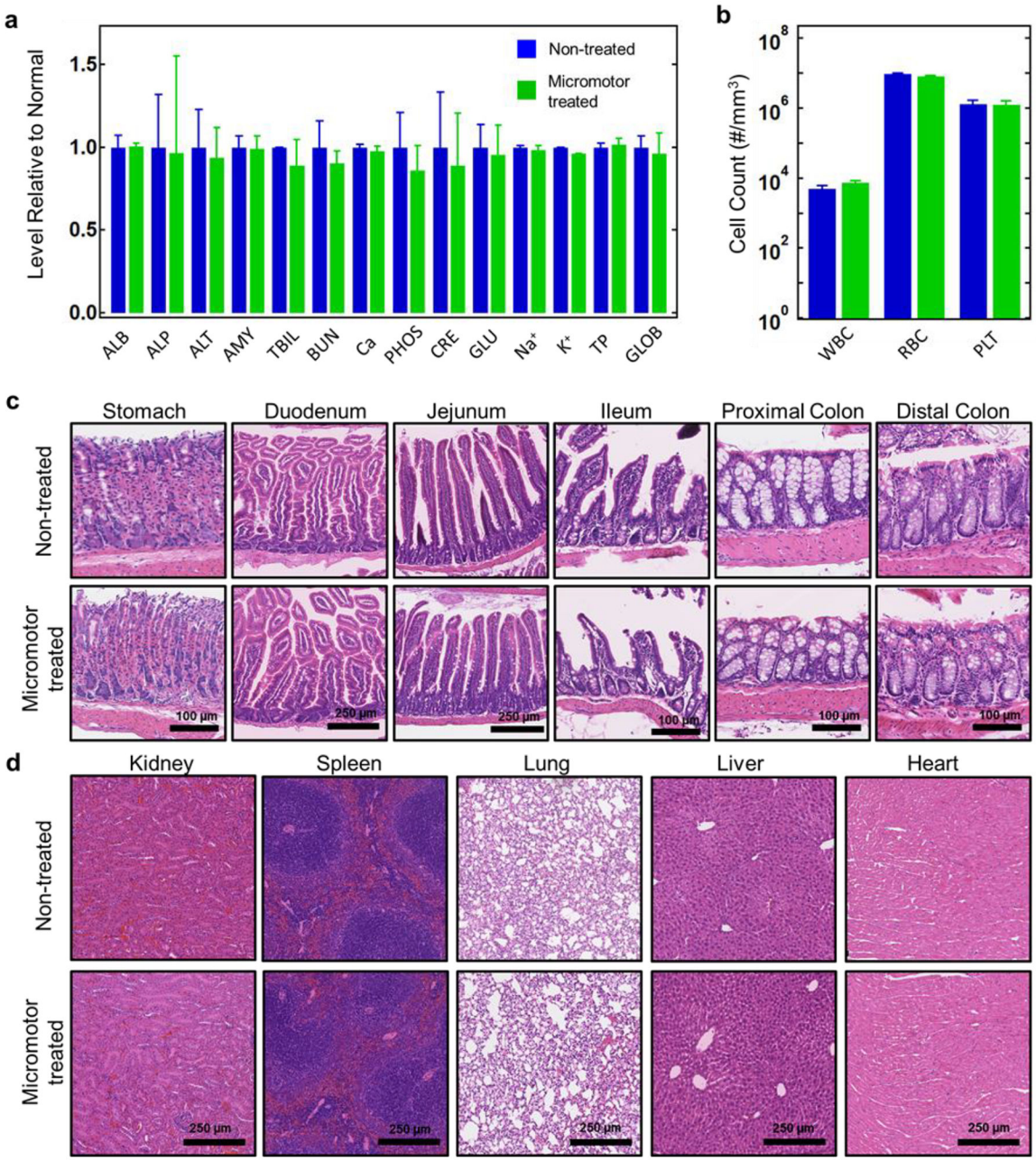

Figure 4.

In vivo evaluation of Fe/Se-loaded micromotor toxicity. a, Comprehensive blood chemistry panel taken from non-treated mice and mice treated for 30 days with Fe/Se-loaded micromotors (n = 3). ALB: albumin; ALP: alkaline phosphatase; ALT: alanine transaminase; AMY: amylase; TBIL: total bilirubin; BUN: blood urea nitrogen; Ca: calcium; PHOS: phosphorus; CRE: creatinine; GLU: glucose; Na^+: sodium; K^+: potassium; TP: total protein; GLOB: globulin (calculated). b, Count of various blood cells taken from non-treated mice and mice treated for 30 days with Fe/Se-loaded micromotors (n = 3). WBC: white blood cells; RBC: red blood cells; PLT: platelets. c, Hematoxylin and eosin (H&E) staining of representative histology sections from different portions of the GI tract from non-treated

mice and mice treated for 30 days with Fe/Se-loaded micromotors. d, H&E staining of representative histology sections of major organs from non-treated mice and mice treated for 30 days with Fe/Se-loaded micromotors. Error bars are defined as mean ± SD.